FRAGILITY ASSESSMENT OF RC BUILDINGS IN SOUTHERN SPAIN BASED ON NEURAL NETWORK PREDICTIONS

J. de-Miguel-Rodríguez[1], M.V. Requena-Garcia-Cruz[2], E. Romero-Sánchez[1], and A. Morales-Esteban[13]

[1] Department of Building Structures and Geotechnical Engineering. University of Seville. Spain
{jdemiguel, eromero13, ame}@us.es

[2] Department of Mechanical Engineering and Industrial Design. University of Cadiz. Spain
mariavictoria.requena@uca.es

[3] Instituto Universitario de Ciencias de la Construcción. University of Seville. Spain

Abstract

The computational burden needed to perform a fragility analysis of structures can be excessive and beyond the capability of regular computing systems. In this work, a Neural Network (NN) implementation is presented to make fragility analyses attainable. Neural Networks allow finding solutions to complex problems at a fraction of the computational time required by conventional analyses. The fragility assessment has been developed for low- and mid-rise 3D buildings located in southern Spain, a moderate earthquake prone area. Nonlinear static analyses are carried out to determine the capacity curves of reinforced concrete buildings, avoiding their specific modelling. The curves are predicted with minimal error, requiring only basic geometric and material parameters of the structures to be specified. Four levels of performance-based seismic design have been considered to assess the seismic performance. Fragility curves have been developed for the structural models with different types of structural configurations and heights. Finally, it should be noted that fragility curves have not been obtained to date for the reinforced concrete buildings of the area.

Keywords: Neural Networks, Fragility Analysis, Reinforced Concrete Structures, Nonlinear Analysis, Multivariate Regression.

1 INTRODUCTION

The seismic hazard of the Mediterranean area is considerable, resulting in cities enduring earthquakes of catastrophic consequences. Such is the case of the 2011 Lorca (Spain) (M_w=4.6) [1], the 2009 L'Aquila (Italy) (M_w=5.8) [2] and the 2012 Emilia (Italy) (M_w=6.1) [3] earthquakes, among others. Despite the progressive development of standards and building codes, it is well known that most of the European building stock predates modern seismic regulations, resulting in a highly potential seismic risk [4]. Hence, there is a strong will, among European countries of this area, to develop new intervention and prevention strategies.

Given this, the use of a method to assess the seismic response of these buildings in a reasonable time and with a good level of accuracy is important [5]. Especially because of the economic cost and time consuming related to the detailed seismic assessment of numerous buildings. Among possible methods to rapidly perform large-scale seismic analyses, Machine Learning techniques such as Neural Networks (NN) stand out. NN allow finding solutions to complex problems at a fraction of the computational time required by conventional analyses. They have been used for solving a wide variety of issues [6], including earthquake engineering related problems. Concerning the seismic analysis, NN have been used to simulate both the linear or nonlinear behaviour of buildings subjected to seismic excitation for the latter damage assessment [7–9]. Also, they have been employed to predict earthquakes series in different countries [10,11].

Large-scale seismic studies are based on determining the average seismic behaviour representative of a given structural typology. This is later considered for the estimation of the seismic vulnerability and damage. However, by considering an average value, a substantial dispersion of the values is entailed. Hence, this can lead to over- or under-estimating the real seismic performance of the building considered. By implementing NN, it is possible to bear in mind all the structural configurations of the buildings and to provide the specific behaviour of the structure under study.

To obtain the seismic behaviour of buildings, it is possible to perform either nonlinear static or dynamic analyses. In the case of nonlinear static analyses, the capacity curve is obtained. In dynamic analyses, other engineering demand parameters are considered such as the floor acceleration or the inter-storey drift [12]. Despite being more accurate, dynamic analyses entail a higher computational burden as well as extensive time consuming for the latter damage assessment. Contrariwise, nonlinear static analyses are conceived as an accurate and robust method for the seismic analysis of low-rise buildings. For the damage assessment, the fragility method is useful and generally accepted among earthquake-experts [13]. Moreover, the computational burden needed to perform a fragility analysis of a large set can be excessive and beyond the capability of regular computing systems. Hence, by implementing the NN for the fragility assessment of buildings, time can be considerably reduced. Neural networks have been employed to estimate fragility directly in [14]. The difference with the current approach, is that by predicting the capacity curves there is a wider scope of application. Apart from deriving fragility curves, which is the specific use-case presented in this paper, other seismic analysis may be facilitated in future work.

Given the above premises, in this work, a NN implementation is presented to make fragility analyses attainable. The fragility assessment has been developed for low- and mid-rise 3D buildings located in southern Spain. This is a moderate earthquake prone area, mainly due to the contact between the Eurasian and African tectonics plates. Among all the building typologies, this work has focused on reinforced concrete (RC) buildings. Many of them were built mainly in the 1970s, before the applications of building and seismic codes. Therefore, they are potentially susceptible to seismic damage as reported in [15–17].

Nonlinear static analyses have been carried out to determine the capacity curves, avoiding their specific modelling. The curves have been predicted with minimal error, requiring only basic geometric and material parameters of the structures to be specified. Four levels of performance-based seismic design have been considered to assess the seismic performance. Fragility curves have been developed for the structural models with different heights and structural configurations. The main novelty of this work is that a novel 'en masse' method is presented for the seismic vulnerability and fragility assessment of urban areas with the accuracy of mechanical methods. Furthermore, according to the authors' knowledge, these results have not been obtained for the RC buildings of the region.

2 METHOD

The method proposed in this paper comprises three main steps. First, a relatively large dataset of building structures (7k samples) is synthetically generated and calculated in SAP2000. The generation of structures is parameterized upon basic geometric variables such as span lengths, beam sizes etc., as shown in Table 1. In a second phase, this dataset is used to extract a training and validation data that will be consumed by a neural network model. After training, the model is capable of predicting the capacity curve of any building within the parameter scope defined in the aforementioned table. Finally, as a third step, fragility curves corresponding to four different damage states are derived from the predicted capacity curves of a broad set of building structures. These structures are divided into 6 groups according their number of stories (two or three), and the relative proportions of their X, Y, Z dimensions. This works represents a step ahead of the contribution originally presented in [18] by the authors.

2.1 Dataset generation (Network Input)

From the parameters listed in Table 1, more than 7k random structures are generated and their corresponding capacity curves are calculated in SAP2000 [19].

Parameter	Minimum Value	Maximum Value	Value Step
Number of spans in X	1	9	1
Number of spans in Y	1	9	1
Number of spans in Z	1	3	1
Dimensions of all spans in X	4 m	8 m	0.166 m
Dimensions of all spans in Y	3 m	6 m	0.125 m
Dimensions of all spans in Z	3 m (a)	3.4 m	0.040 m
Height of suspended ground floor	0.6 m	0.8 m	0.025 m
Load-bearing beams: width	30 cm	60 cm (b)	- (c)
Load-bearing beams: height	30 cm	60 cm	- (c)
Non-load-bearing beams: width	30 cm	30 cm	- (c)
Non-load-bearing beams: height	25 cm	30 cm	- (c)
Supports: width in X	30 cm	30 cm	- (c)
Supports: width in Y	30 cm	30 cm	- (c)
Slab thickness	25 cm	30 cm	- (c)

Table 1: Parameters for random generation of structures. Note: (a) Ground floor height is always 3.4 m. (b) Wide load-bearing beams are randomly considered when the span length is shorter than 6 m. (c) Frames dimensions are first calculated according to their span, then, the most restrictive section for each type (load-bearing, non-load-bearing, supports, slabs) is used for the whole structure.

Within the parameter scope defined in the above schema, the total (T) number of possible samples can be expressed by the following formula:

$$T = n_x \cdot n_y \cdot n_z \cdot (s_x)^{nx} \cdot (s_y)^{ny} \cdot (s_z)^{nz} \tag{1}$$

Where n_x, n_y, n_z = the number of spans in X, Y and Z, and s_x, s_y, s_z = the number of steps in X, Y and Z. By Applying the values used for the generation of the dataset, then $T = 9 \times 9 \times 3 \times 24^9 \times 24^9 \times 10^3$ and therefore, $T > 10^{18}$. This accounts for the vast variety of samples that fall under the parameter scope and justifies the random sampling used to create the dataset. A selection of the resulting capacity curves calculated is presented in Figure 1.
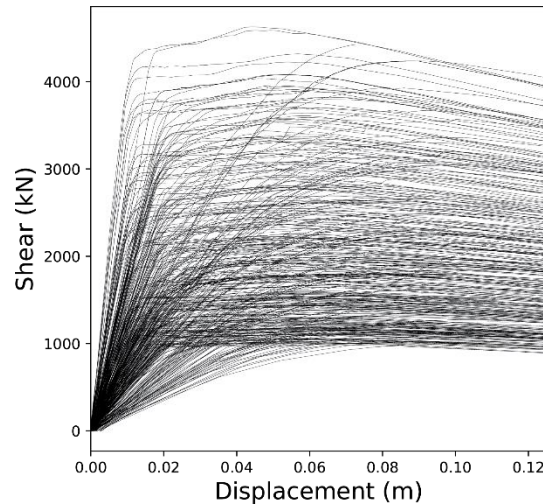

Figure 1: Capacity curves created from 7k buildings randomly selected.

2.2 Nonlinear static analyses (Network output)

Different models of 3D RC structures have been developed considering the input parameters and limits. The concentrated plasticity approach has been used for the nonlinear modelling of the RC frames. The typical model of a plastic hinge for each structural component is used following the prescriptions presented in [20]. The rigid diaphragm effect has been also borne in mind. The loads considered in the analysis have been: self-weight of all the elements; additional dead loads (slabs, roofs and ceilings); and, a permanent live load. They have been combined in different hypotheses as presented in [18]. All the models have been fixed-based. The horizontal load pattern has been calculated proportional to the masses and to the height of each of the models.

2.3 Artificial Neural Network

The main aspects of a neural network model are: (i) the input and output layers, (ii) the number and structure of the hidden layers, (iii) the activation functions of each layer and (iv) the optimization process and associated parameters.

As expected, the input layer coincides roughly with the parameter set used for the generation of the dataset. There is a total of 30 parameters, 9 for each possible span in X and another 9 for Y, 5 in Z (including the service floor), plus 2 dimensions for bearing beams, 2 for non-bearing beams; and another 2 for supports and 1 for the slab height.

For the output layer, the objective is to arrive at a layer size that, on the one hand, is large enough to provide a detailed representation of the capacity curves and, on the other hand, that it is not too large that it compromises the accuracy of the model. The best results in this regard were achieved with an output layer size of 100 and the same results were obtained with 135 neurons (Table 2). For simplicity, an output size of 100 neurons has been selected, which has enough resolution to convey a detailed account of the capacity curves.

Network Architecture					
Layer scheme and size				MAE loss	
X	h1	h2	Y	Validation error	Training error
30	65	65	65	0.0127	
30	65	65	82	0.0127	0.0105
30	65	65	100	0.0126	0.0106
30	65	65	135	0.0130	
30	65	100	135	0.0126	0.0107

Table 2: Testing different output layer sizes.

With regards to the hidden layers, the model was quickly able to achieve a mean absolute error (MAE) of 0.0126 with only two hidden layers (h_1, h_2). Adding a third layer produced less optimal results with clear overfitting. The same goes for a single hidden layer, except without overfitting. After testing a number of hidden layer numbers and sizes (Table 3), the final architecture selected was X-h_1-h_2-Y = 30-65-65-100.

Network Architecture					
Layer scheme and size				MAE loss	
X	h_1		Y	Validation error	Training error
30	30		100	0.0153	
30	65		100	0.0135	
30	100		100	0.0132	
30	135		100	0.0131	0.0115
30	170		100	0.0132	
30	205		100	0.0133	
X	h_1	h_2	Y	Validation error	Training error
30	30	30	100	0.0133	
30	30	65	100	0.0137	
30	30	100	100	0.0137	
30	55	80	100	0.0128	
30	**65**	**65**	**100**	**0.0126**	**0.0106**
30	65	100	100	0.0131	
30	100	100	100	0.0134	
X	h_1	h_2	h_3	Y	Validation error	Training error
30	30	30	30	100	0.0137	
30	30	30	65	100	0.0133	0.0107
30	30	65	65	100	0.0138	
30	65	65	65	100	0.1407	

Table 3: Final architecture selected.

Activation functions considered in this model were narrowed down to ReLU (Rectified Linear Unit), sigmoid and tanh (hyperbolic tangent), after preliminary testing. Sigmoid activation is typically used for the output layer as it maps values from 0 to 1. For the hidden layers, ReLU is a common choice in deep learning [21], while tanh has been previously used to address similar prediction problems [22]. Further testing determined the choice of tanh over ReLu, in hidden layers. Finally, Table 4 presents the main parameters tested for the error optimization process and their results.

Parameter Variation	MAE Loss (1200 epochs)	
	Validation error	Training error
Initial conditions (no variation)	0.0126	0.0103
Adadelta (instead of SGD)	0.0136	0.0114
SGD without Nesterov (M = 0.9)	0.0128	0.0107
Lr (Learning rate) = 0.25	0.0128	0.0110

Lr (Learning rate) = 0.45	0.0127	0.0106
Decay = Lr/(6·ep)	0.0127	0.0108
Decay = Lr/(10·ep)	0.0128	0.0106
Sigmoid activation in hidden layers	0.0147	0.0130
Relu activation in hidden layers	0.1406	0.1358
Batch size = 1 (minimum)	0.0131	0.0102
Batch size = 6	0.0129	0.0102
Batch size = 24	0.0124	0.0103
Batch size = 36	0.0131	0.0114

Table 4: Main parameters tested for the error optimization process and their results.

Once all the aspects that lead up to the complete definition of the network have been settled, the model is ready for training. In Table 5, a summary of the complete configuration of the network model is provided.

Network Architecture				
Layers	X	h_1	h_2	Y
Layer size	30	65	65	100
Network Parameters				
Layers	X	h_1	h_2	Y
Activation	-	tanh	tanh	sigmoid
Weight initialization	-	Random (0, 0.1)	Random (0, 0.1)	Random (0, 0.1)
Bias initialization	-	Random (0, 1)	Random (0, 1)	Random (0, 1)
Training Parameters				
Lr (Learning rate)	0.35			
Decay	Lr/(8.ep)			
M (Momentum)	Nesterov			
Epochs	1200			
Batch size	24			
Shuffle samples at each epoch	Yes			

Table 5: Configuration of the network model.

2.4 Fragility analysis

The method proposed considers the assessment of fragility functions using a building-based damage assessment methodology. A fragility function determines the probability of an engineering parameter not exceeding a certain threshold [23]. In this work, this parameter is the total roof displacement and its thresholds will be derived from a damage assessment method [24]. In statistical terms, a fragility curve is the cumulative distribution function (CDF) of a random variable (x):

$$F_X(x) = P(X \leq x) \tag{1}$$

A CDF is built from the probability density function (PDF) of that random variable. The CDF is calculated as the area covered by the PDF in between two values (a, b) of the distribution variable. In generic terms, given any PDF, the CDF can be obtained as:

$$F_X(x) = \int_a^b f_X(t)d_t \tag{2}$$

This integral is not always solvable mathematically due to potential intractability of the PDF. For this reason, and also because of simplicity, many areas aside from seismic engineering work with data that fits a well-known distribution (if possible, a normal distribution). In seismic

studies, the probability density function is often elaborated upon an incremental dynamic analysis of a single building [25]. In some cases, this single building is used as a prototype to assess the fragility of multiple buildings that share very common characteristics and thus, similar demand values are expected [26]. The distribution obtained tracks either the inter-storey drift or the peak ground acceleration, and the experimental samples typically do not follow a normal distribution but a lognormal one (which is slightly harder to integrate but has extensive literature available on the same). In the present method, however, there are important differences. On the one hand the engineering demand parameter is set as the total roof displacement. Then, on the other hand, and most importantly, the random variable (total roof displacement) is not generated by multiple experiments over a same building but by a large number of them. The implications of this setup are (i) distributions might neither follow a normal nor a lognormal pattern, as in the aforementioned studies. This translates in the impossibility of providing an analytical solution for the CDF and a computational estimation will be provided instead. And (ii) linear regressions over the distribution, as carried out in [26,27], may display very large variance and/or extreme slope angles, which would in turn yield these methods inapplicable.

In summary, the CDF in this study is computationally approximated as the area of a probability density curve calculated upon the distribution of the roof displacements of multiple buildings. For the calculation of the curve points, the kernel density estimation method of the Python library SciKit-Learn [28] has been employed. Regarding the roof displacements, four different discretized damage states (DS) are considered at global building level: the immediate occupancy (DS1), damage control (DS2), life safety (DS3) and collapse prevention (DS4). The equations (Eq. (3)) provided in [29] have been considered to define each DS. As pointed out in this work, the threshold of each damage state for the global behaviour of a building is defined at the step when the first structural computed (wall or column) attains a certain damage state.

$$S_{ds1} = S_{dy}$$
$$S_{ds2} = 1.5S_{dy}$$
$$S_{ds3} = 0.5(S_{dy} + S_{du}) \quad\quad (3)$$
$$S_{ds4} = S_{du}$$

The values (S_{dy}, S_{du}) are obtained from the capacity curves predicted by the neural network model following the N2-method established in the Eurocode-8 part-1 (EC8-1) [30]. This procedure provides the calculation of the idealized bilinear capacity curve, which requires the mapping of multi-degree-of-freedom (MDOF) curves to those of their equivalent single-degree-of-freedom (SDOF) system. This has been carried out through the transformation factor (Γ). This factor has been computed by considering the modal shapes as normalized triangular patterns. These have been computed according to the masses of each of the control nodes of the floors. After this procedure, the yielding (d_y) and the ultimate (d_u) displacements have been obtained for each RC structure. In this case, the d_u has been computed as the 80% decay of the peak strength of the capacity curve, as suggested in the Eurocode-8 part-3 [31]. And d_y as the 'elbow' point of the idealized bilinear capacity curve following the N2-method.

2.5 Data exploration

Once the four damage states are obtained for each SDOF-equivalent capacity curve, a point-cloud of these values can be generated for all buildings, as presented in Figure 2(a). One of the first aspects that stands out from this chart, is that the trends of the distributions for the different damage states are manifestly vertical (except perhaps for DS4 which presents a much wider

variance of displacements). Regression estimations on each damage state result in regression lines at almost 90º (+/- 2%). Indeed, due to the broad range of building sizes being considered, there is in turn, a wide range of shear capacity present among them. In Figure 2(b), a graph of shear capacity to building mass is presented, showing a direct correlation between them. However, it is interesting that the displacements are in general, not critically affected by the structural mass.
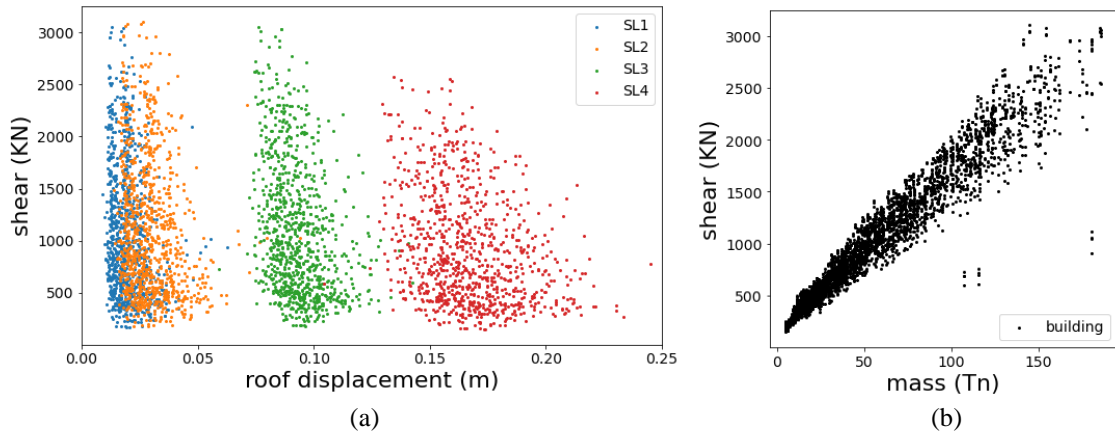

Figure 2: (a) Shear-displacement plot representing all damage states for all buildings. (b) Shear-mass correlation for all buildings.

Another important aspect that may be observed in Figure 2(a) is that the points corresponding to DS1 and DS2 overlap substantially. The main reason is that both two- and three-storey buildings are considered simultaneously. Since roof displacement is the variable being monitored, wide variations are expected when aggregating data from buildings with a very important relative difference in the number of floors. When looking at the same data plot but grouping buildings by their number of storeys, a cleaner segregation of samples is obtained for DS1 and DS2 as shown in Figure 3(a) and (b).
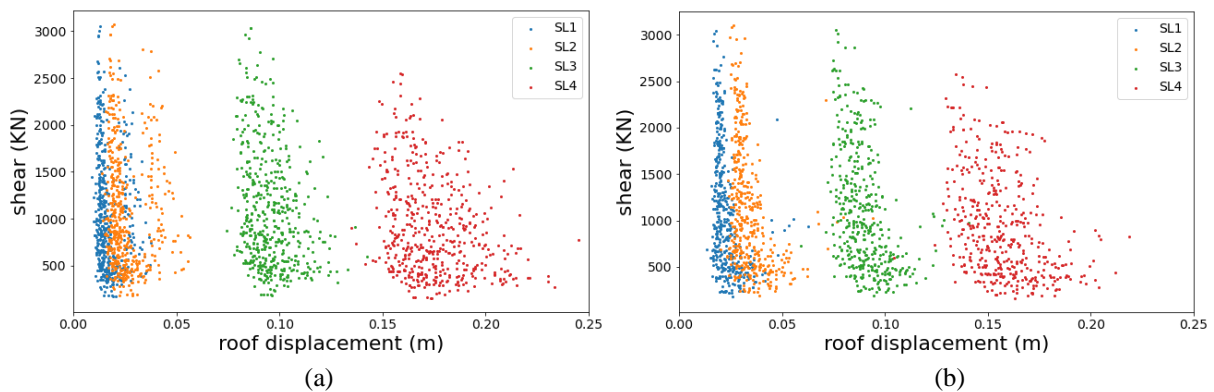

Figure 3: Shear-displacement plot representing all damage states for (a) two- and (b) three-storey buildings.

Despite having achieved a cleaner cut between DS1 and DS2 by separating the buildings in groups according to their number of storeys, some strong overlaps are still noticeable especially in the group of two-storey buildings. It is quite visible in Figure 3(a), that for the aforementioned damage states, there are two distinct vertical clusters, a dense one (to the left) and another one slightly coarser to the right. The primary driver behind this polarization, resulting in two different clusters, is explained, above all, by the differences in the structural typology of the samples. In particular, the less dense clusters, (sliding to the right – featuring greater

displacements) for both DS1 and DS2 are mostly characterised by buildings with wide beams instead of deep beams and slightly thinner slabs (25 cm vs. 30 cm). To illustrate the impact of wide vs. deep beams on the total roof displacement for each damage state, Figure 4 and Figure 5 present a graphic account of these values according to their beam type.
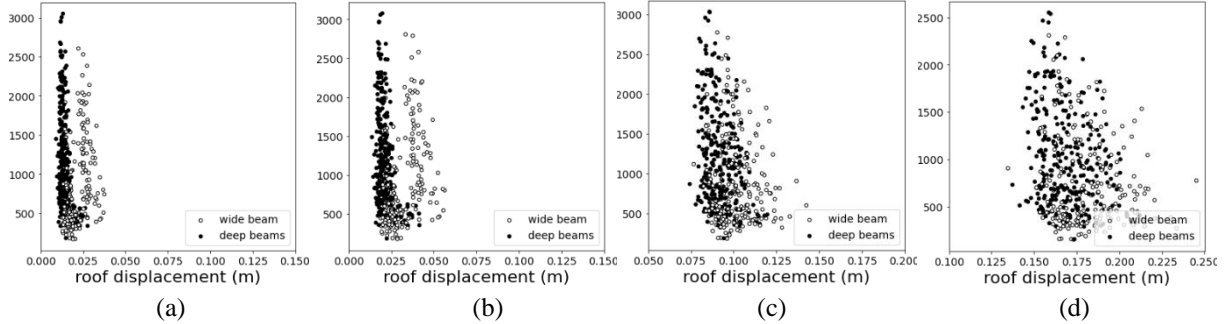

Figure 4: DS1 (a), DS2 (b), DS3 (c) and DS4 (d) of two-storey structures with wide and deep beams.
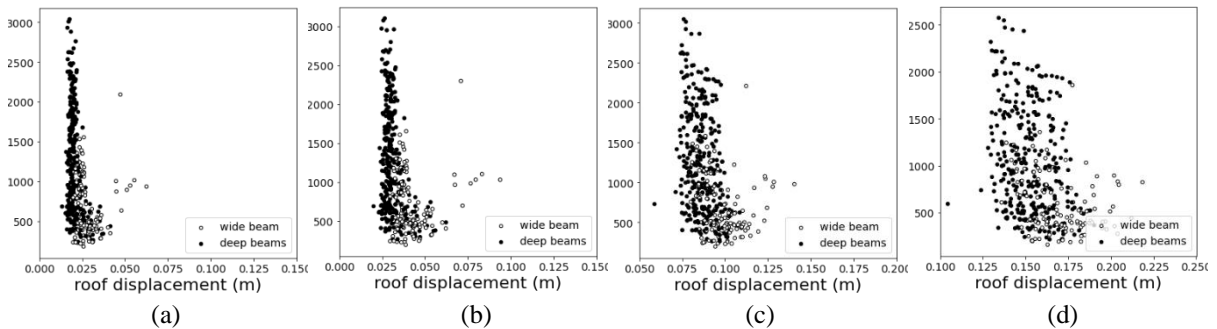

Figure 5: DS1 (a), DS2 (b), DS3 (c) and DS4 (d) of three-storey structures with wide and deep beams.

According to the insights acquired through the exploration of the data presented, the initial dataset of buildings will be divided into the following four groups for the purpose of fragility analysis:

- [2_storey_deep_beam] Two-storey buildings with deep beams and 30 cm slabs.
- [2_storey_wide_beam] Two-storey buildings with wide beams and 25 cm slabs.
- [3_storey_deep_beam] Three-storey buildings with deep beams and 30 cm slabs.
- [3_storey_wide_beam] Three-storey buildings with wide beams and 25 cm slabs.

3   RESULTS

After training the neural network model described in the Method section, the average validation mean absolute error (MAE) over 60 random trials and 1200 epochs was 0.0124 (1.24%). The MAE distribution is graphed in Figure 6(a), and a visual comparison of a predicted vs. validation capacity curve corresponding to a sample with an absolute error equal to the mean, is graphed in Figure 6(b). The root mean square error (RMSE) was also calculated yielding a value of 0.0134 and following a very similar distribution to the MAE, while the overfitting ratio remained contained at 0.904.

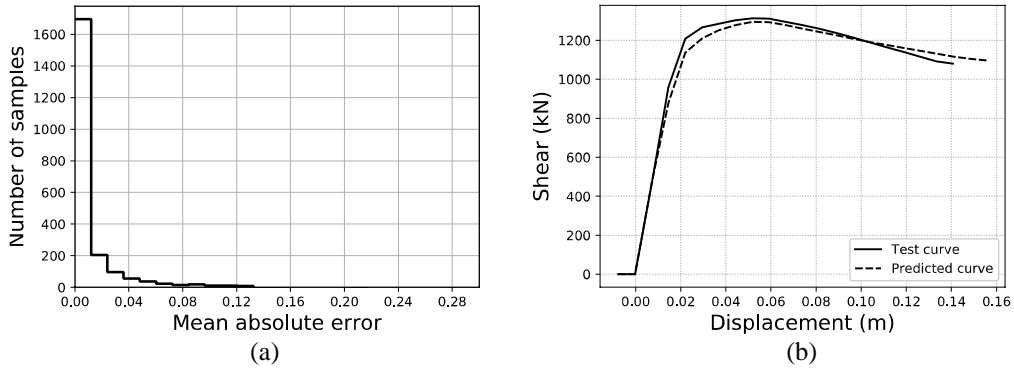(a)   (b)

Figure 6: (a) Distribution of the mean absolute error (MAE) and (b) Predicted curve vs. validation curve for a sample corresponding approximately to the mean absolute error in the distribution (0.0124).

With regards to the fragility analysis, the methodology laid out above is applied to the four groups defined in the data exploration section. Consequently, probability density and fragility curves (cumulative distribution curves) are obtained for each group. These are presented in Figure 7, Figure 8, Figure 9 and Figure 10.
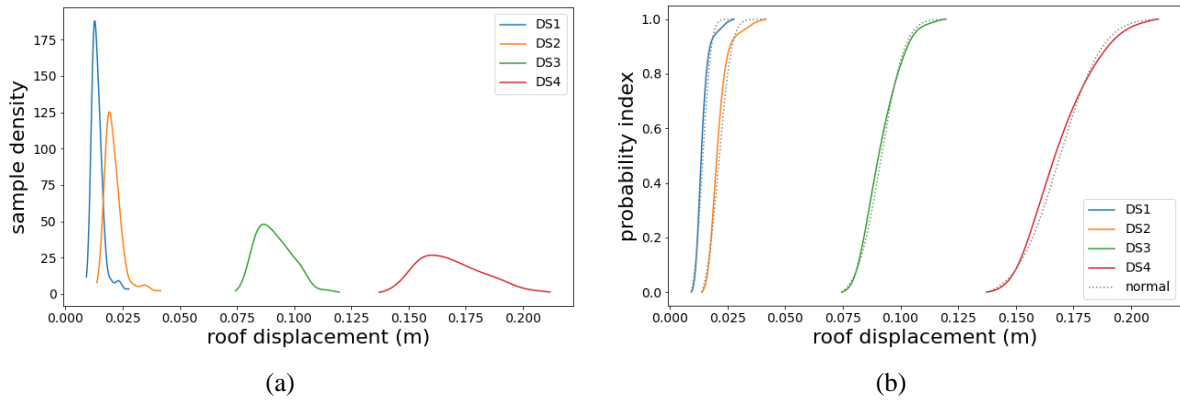

(a)   (b)

Figure 7: probability density (a) and cumulative distribution (b) functions of deep beams two-storeys structures.

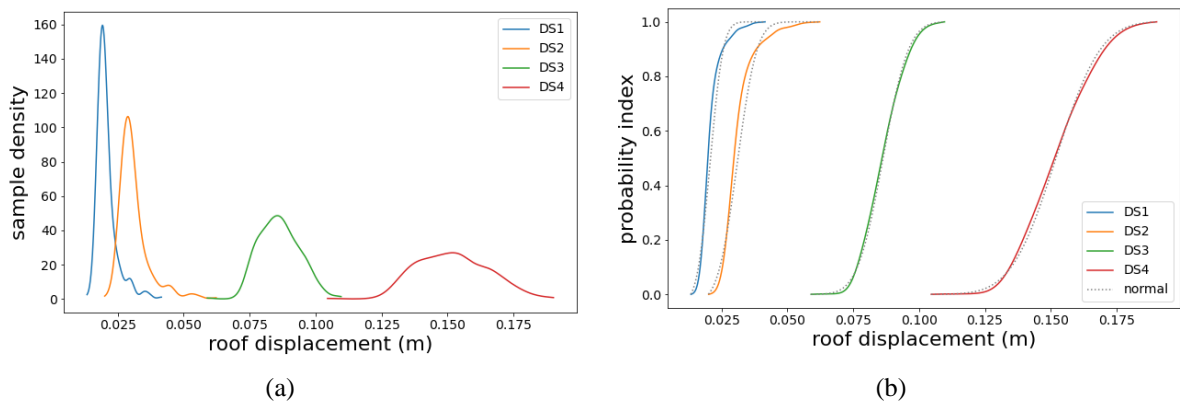(a)   (b)

Figure 8: probability density (a) and cumulative distribution (b) functions of deep beams three-storeys structures.

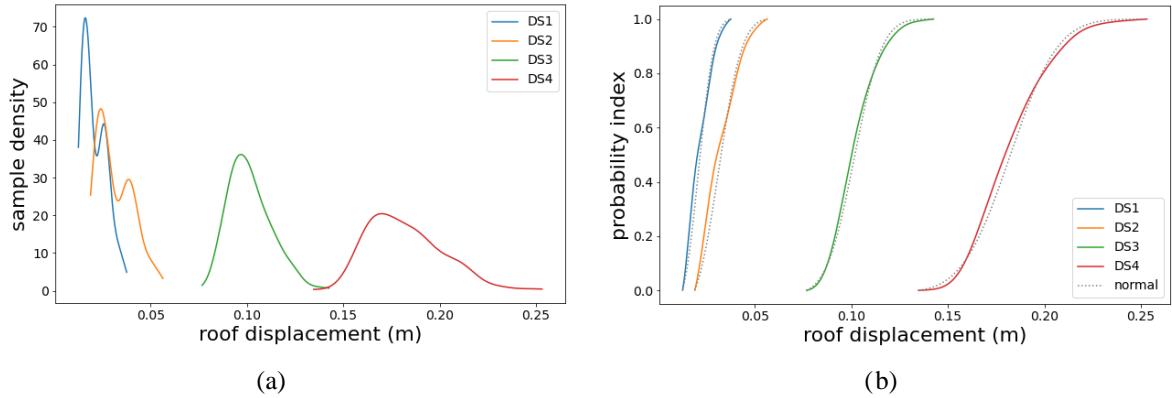(a)   (b)

Figure 9: probability density (a) and cumulative distribution (b) functions of wide beams two-storeys structures.

(a)   (b)
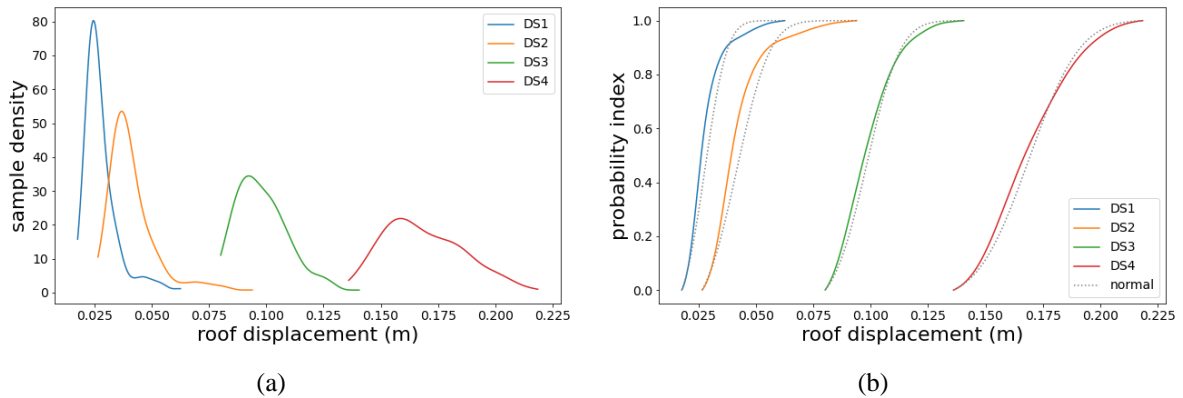
Figure 10: probability density (a) and cumulative distribution (b) functions of wide beams three-storeys structures.

4   DISCUSSION

Although this research is centered on its applicability to a very broad range of structures, the results achieved by the neural network model still compare quite well to other similar works [32,33]. Overall, these results have been possible mainly because of the relatively large size of the training set. In early experiments (not mentioned in this paper) the training set was limited to 2k samples and the model failed to predict the curves with sufficient accuracy. In this sense, enlarging the dataset to 7k samples has been by far the driver of the greatest impact among all other parameters and design decisions made around the model. Despite the success of the predictions, it must be noted that the results must be cross-checked with actual buildings, to assess among other things, the suitability of the modeling assumptions put forth in this work, e.g.: absence of infills or uncertainties pertaining to the nature of the building materials.

The fragility analysis, implemented upon the capacity curves predicted by the neural network model, provides insights for the buildings selected that allow a better understanding in terms of their seismic performance. The buildings selected yield close-to-normal distributions for all the damage states. The major exception has been the group of two-storey structures with wide beams. In this group, a double 'camel-hump' is easily observed. This might be due to the variable width of the beams, as this ranges from 30 cm to 60 cm. More analysis should be carried out to pin-point the exact cause. Three-storey buildings present considerably higher probability of collapse for lower displacements, increasing up to 30%. For DS1, DS2 and DS3 the results are rather similar. Structures with wide beams present a higher probability of damage. As it can be observed, for DS1 and DS2, the displacement ranges from 0 to 5 cm. However, for wide beams buildings, these levels range from 0 to 25 cm. This is even more

severe for buildings with two storeys instead of three. For two-storey buildings in DS3, the 50% probability of exceedance corresponds to a 10 cm displacement in the case of wide beams, while with deep beams it is reduced to 8 cm. These differences are even higher for DS4, where displacement ranges from 12.5 to 22.5 cm in wide beams, compared to 10-20 cm for deep beams. However, three-storey buildings do not present substantial differences between wide and deep beam buildings for either DS3 or DS4.

5 CONCLUSIONS

This paper presented the implementation of a NN-based fragility analysis of low-rise 3D RC buildings located in southern Spain. The main conclusions of this work are enumerated below:

- This study provided an 'en masse' method for the seismic vulnerability and fragility assessment of large-scale analysis with the accuracy of mechanical methods.

- The fragility curves showed that taller buildings tend to present a higher probability of damage compared to lower buildings. Damage can be increased up to 30% if only one storey is added to the structure.

- Structures with wide beams present a higher probability of damage.

This work represented the first attempt in massively assessing the seismic fragility of low-rise RC buildings of the region under study. In future work the scope of buildings should be extended by: (i) increasing the number of storeys in the neural network model; (ii) including irregularities such as balconies, patios, and infills; and, (iii) performing the analyses carried out in this work in a dynamic nonlinear fashion such as incremental dynamic analysis.

ACKNOWLEDGEMENTS

REFERENCES

[1]   M. Feriche, F. Vidal, G. Alguacil, C. Aranda, J. Pérez-Muelas, M. Navarro, et al. Performance of cultural heritage of Lorca (Spain) during the two small earthquakes of May 11th, 2011 . 11th World Conference on Earthquake Engineering, Lisbon: 2021.

[2]   Lagomarsino S. Damage assessment of churches after L'Aquila earthquake (2009). Bulletin of Earthquake Engineering 2012;10:73–92. https://doi.org/10.1007/s10518-011-9307-x.

[3]   Cattari S, Degli Abbati S, Ferretti D, Lagomarsino S, Ottonelli D, Tralli A. Damage assessment of fortresses after the 2012 Emilia earthquake (Italy). Bulletin of Earthquake Engineering 2014;12:2333–65. https://doi.org/10.1007/s10518-013-9520-x.

[4]   Tsionis G, Palermo V, Sousa ML. Building stock inventory to assess seismic vulnerability across Europe - Publications Office of the EU. 2019.

[5]   Stefanini L, Badini L, Mochi G, Predari G, Ferrante A. Neural networks for the rapid seismic assessment of existing moment-frame RC buildings. International Journal of Disaster Risk Reduction 2022;67:102677. https://doi.org/10.1016/j.ijdrr.2021.102677.

[6]   Estêvão J. Feasibility of Using Neural Networks to Obtain Simplified Capacity Curves for Seismic Assessment. Buildings 2018;8:151. https://doi.org/10.3390/buildings8110151.

[7]   Chakraverty S, Gupta P, Sharma S. Neural network-based simulation for response identification of two-storey shear building subject to earthquake motion. Neural Comput Appl 2010;19:367–75. https://doi.org/10.1007/s00521-009-0279-6.

[8]   Vazirizade SM, Nozhati S, Zadeh MA. Seismic reliability assessment of structures using artificial neural network. Journal of Building Engineering 2017;11:230–5. https://doi.org/10.1016/J.JOBE.2017.04.001.

[9]   Mitropoulou C, Papadrakakis M. Developing fragility curves based on neural network IDA predictions. Eng Struct 2011;33:3409–21. https://doi.org/10.1016/j.engstruct.2011.07.005.

[10]   Reyes J, Morales-Esteban A, Martínez-Álvarez F. Neural networks to predict earthquakes in Chile. Applied Soft Computing Journal 2013;13:1314–28. https://doi.org/10.1016/j.asoc.2012.10.014.

[11]   Zhang GP, Qi M. Neural network forecasting for seasonal and trend time series. Eur J Oper Res 2005;160:501–14. https://doi.org/10.1016/j.ejor.2003.08.037.

[12]   Requena-Garcia-Cruz MV, Romero-Sánchez E, Morales-Esteban A. Numerical investigation of the contribution of the soil-structure interaction effects to the seismic performance and the losses of RC buildings. Developments in the Built Environment 2022;12:100096. https://doi.org/10.1016/j.dibe.2022.100096.

[13]   Maio R, Tsionis G. Seismic fragility curves for the European building stock: Review and evaluation of analytical fragility curves. 2016. https://doi.org/10.2788/586263.

[14]   Wang Z, Pedroni N, Zentner I, Zio E. Seismic fragility analysis with artificial neural networks: Application to nuclear power plant equipment. Eng Struct 2018;162:213–25. https://doi.org/10.1016/J.ENGSTRUCT.2018.02.024.

[15]   Requena-Garcia-Cruz MV, Morales-Esteban A, Durand-Neyra P. Assessment of specific structural and ground-improvement seismic retrofitting techniques for a case study RC building by means of a multi-criteria evaluation. Structures 2022;38:265–78. https://doi.org/10.1016/j.istruc.2022.02.015.

[16]   Requena-Garcia-Cruz MV, Morales-Esteban A, Durand-Neyra P. Optimal ductility enhancement of RC framed buildings considering different non-invasive retrofitting techniques. Eng Struct 2021;242:112572. https://doi.org/10.1016/j.engstruct.2021.112572.

[17]   Requena-García-Cruz MV, Morales-Esteban A, Durand-Neyra P, Estêvão JMC. An index-based method for evaluating seismic retrofitting techniques. Application to a reinforced concrete primary school in Huelva. PLoS One 2019;14:e0215120. https://doi.org/10.1371/journal.pone.0215120.

[18]   de-Miguel-Rodríguez J, Morales-Esteban A, Requena-García-Cruz M-V, Zapico-Blanco B, Segovia-Verjel M-L, Romero-Sánchez E, et al. Fast Seismic Assessment of Built Urban Areas with the Accuracy of Mechanical Methods Using a Feedforward Neural Network. Sustainability 2022;14:5274. https://doi.org/10.3390/su14095274.

[19]   Computers and Structures INC. SAP2000 Users' Manual 2014.

[20]   Federal Emergency Management Agency (FEMA). FEMA-440: Improvement of nonlinear static seismic analysis procedures. vol. 440. United States: 2005.

[21]   Krizhevsky A, Sutskever I, Hinton GE. ImageNet classification with deep convolutional neural networks. Commun ACM 2017;60:84–90. https://doi.org/10.1145/3065386.

[22] da S. Gomes GS, Ludermir TB, Lima LMMR. Comparison of new activation functions in neural network for forecasting financial time series. Neural Comput Appl 2011;20:417–39. https://doi.org/10.1007/s00521-010-0407-3.

[23] Kennedy RP, Cornell CA, Campbell RD, Kaplan S, Perla HF. Probabilistic seismic safety study of an existing nuclear power plant. Nuclear Engineering and Design 1980;59:315–38. https://doi.org/10.1016/0029-5493(80)90203-4.

[24] European Union. Eurocode 8: Design of structures for earthquake resistance. Part 1: General rules, seismic actions and rules for buildings. Brussels: 2004.

[25] Zentner I, Gündel M, Bonfils N. Fragility analysis methods: Review of existing approaches and application. Nuclear Engineering and Design 2017;323:245–58. https://doi.org/10.1016/J.NUCENGDES.2016.12.021.

[26] Milutinovic Z v., Trendafiloski GS. WP4:Vulnerability of current buildings. Risk-UE project Handbook. European Comission 2003. https://doi.org/10.1007/978-1-4020-3608-8_23.

[27] Zentner I, Humbert N, Ravet S, Viallet E. Numerical methods for seismic fragility analysis of structures and components in nuclear industry - Application to a reactor coolant system. Georisk 2011;5:99–109. https://doi.org/10.1080/17499511003630512.

[28] scikit-learn: machine learning in Python — scikit-learn 1.2.1 documentation n.d. https://scikit-learn.org/stable/ (accessed February 27, 2023).

[29] Lagomarsino S, Giovinazzi S. Macroseismic and mechanical models for the vulnerability and damage assessment of current buildings. Bulletin of Earthquake Engineering 2006;4:415–43. https://doi.org/10.1007/s10518-006-9024-z.

[30] European Union. Eurocode 8: Design of structures for earthquake resistance. Part 1: General rules, seismic actions and rules for buildings. Belgium: 2004.

[31] European Union. Eurocode-8: Design of structures for earthquake resistance. Part 3: Assessment and retrofitting of buildings. Brussels, Belgium: 2005.

[32] Morfidis K, Kostinakis K. Approaches to the rapid seismic damage prediction of r/c buildings using artificial neural networks. Eng Struct 2018;165:120–41. https://doi.org/10.1016/J.ENGSTRUCT.2018.03.028.

[33] Perez-Ramirez CA, Amezquita-Sanchez JP, Valtierra-Rodriguez M, Adeli H, Dominguez-Gonzalez A, Romero-Troncoso RJ. Recurrent neural network model with Bayesian training and mutual information for response prediction of large buildings. Eng Struct 2019;178:603–15. https://doi.org/10.1016/j.engstruct.2018.10.065.